Suspended Large-Area MEMS-Based Optical Filters for Multispectral Shortwave Infrared Imaging Applications

Dhirendra Kumar Tripathi, *Member, IEEE*, Fei Jiang, Ramin Rafiei, K. K. M. B. Dilusha Silva, *Member, IEEE*, Jarek Antoszewski, Mariusz Martyniuk, *Member, IEEE*, John M. Dell, *Member, IEEE*, and Lorenzo Faraone, *Senior Member, IEEE*

***Abstract*— We present the design, fabrication, and optical and mechanical characterization of silicon-/silicon-oxide-based optical filters and distributed Bragg reflectors in sizes ranging from 500 μm × 500 μm to 5 mm × 5 mm. They are designed to be used in conjunction with either single-element photodetectors or large-area focal plane arrays to realize tunable multispectral sensors or adaptive focal plane arrays in the shortwave infrared wavelength range. Surface optical profile measurements indicate a flatness of the order of 30 nm in the fabricated structures across several millimeters. Single-point spectral measurements on devices show an excellent agreement with simulated optical models, and demonstrate Si-SiO_x-Si fixed optical filters with a 94% transmission at 1940 nm with a full-width at half-maximum of 250 nm. Distributed Bragg reflectors demonstrate 90% reflectance across the 1560–2050-nm wavelength range, making them suitable as broadband reflectors. The optical spatial uniformity across a 3-mm × 3-mm device shows only a 3% variation across the entire optically active area. Finally, the mechanical resonance characteristic of a 1-mm × 1-mm fabricated device shows the lowest resonant frequency of the suspended structure to be 39 kHz, indicating excellent immunity to extraneous low-frequency vibrations. [2014-0278]**

***Index Terms*— Distributed Bragg reflector, Fabry-Perot, optical filter, focal plane array, shortwave infrared.**

I. Introduction

WITH THE advent of large-area two-dimensional focal plane array (FPA) detectors from the near infrared (NIR) to the long wave infrared (LWIR) wavelengths (0.7 μm to 20 μm), it is now possible to image over a very large region of the infrared spectrum. Among the reported FPA technologies, InGaAs based FPAs can be operated at room temperature while covering the visible to shortwave infrared (SWIR, up to 2.5 μm) wavelength range. These FPAs are now part of many commercial NIR and SWIR spectroscopic imaging systems [1]–[4]. Although originally developed for defense, security and aerospace applications, such imaging systems have found new applications in crop germination studies, drug quality analysis, and food security and quality analysis [5]–[10]. The combination of tunable optics with an FPA can provide new capabilities, such as the wavelength selective FPA or so-called adaptive FPA. In traditional spectroscopic imaging systems, this function is achieved by passing the incident spectrum through a series of complex optical components, and then onto the FPA [11]. These traditional systems offer high resolution and a wide operating wavelength range. However, such systems are expensive, bulky, fragile, and not readily field-portable. With recent advances in microelectromechanical systems (MEMS), miniature, highly-portable, robust, and low-cost spectroscopic systems have become a reality [12]–[16]. These systems replace the bulky and fragile optics components of traditional systems with MEMS-based miniature filters and mirrors. The integration of a MEMS-based Fabry-Perot tunable filter with the detector can result in a very compact spectrometer, and an array of such compact spectrometers can be used to provide individual on-pixel spectroscopy in an adaptive FPA.

Our past work attempted monolithic integration of the detector with a MEMS-based filter to create multispectral detectors at SWIR wavelengths [17], [18]. Other research groups have proposed resonant cavity enhanced detector structures by growing the detector on top of one of the filter mirrors for the mid-wave infrared (MWIR) wavelength range [19], [20]. With monolithically integrated approaches, one is limited by the choice of materials compatible with both the FPA and the MEMS-based tunable filter fabrication. Furthermore, monolithic integration cannot take full advantage of the myriad of available processes to optimize the stress and optical properties that are available exclusively to MEMS technologies, and the many optimization technologies available exclusively for detector fabrication.

Manuscript received September 8, 2014; revised November 11, 2014; accepted November 30, 2014. Date of publication January 25, 2015; date of current version July 29, 2015. This work was supported in part by the Grains Research and Development Corporation, in part by the Australian Research Council, in part by the Western Australian State Government Office of Science, and in part by the Western Australian Node through the Australian National Fabrication Facility, a company established under the National Collaborative Research Infrastructure Strategy to provide nano and microfabrication facilities for Australian researchers. Subject Editor S. Merlo.

D. K. Tripathi, R. Rafiei, K. K. M. B. D. Silva, J. Antoszewski, M. Martyniuk, J. M. Dell, and L. Faraone are with the School of Electrical, Electronics, and Computer Engineering, University of Western Australia, Perth, WA 6009, Australia (e-mail: dhirendra.tripathi@research.uwa.edu.au; ramin.rafiei@uwa.edu.au; dilusha.silva@uwa.edu.au; jarek.antoszewski@uwa.edu.au; mariusz.martyniuk@uwa.edu.au).

F. Jiang is with MRX technologies, West Perth, WA 6005, Australia (e-mail: floyd.jiangfei@gmail.com).

Color versions of one or more of the figures in this paper are available online at http://ieeexplore.ieee.org.

Digital Object Identifier 10.1109/JMEMS.2014.2385081

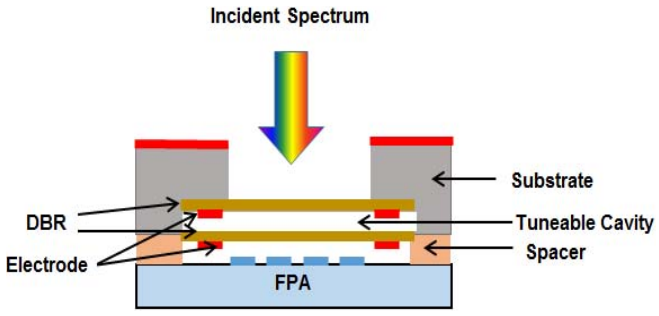

Fig. 1. Working principle of proposed module consisting of a tunable Fabry-Perot cavity hybrid bonded to a detector or imaging FPA.

These limitations can be overcome by a hybrid approach, where the detector and MEMS-based optics are fabricated and optimized separately and bonded together with the help of spacer/bonding pads. Neumann *et. al.* [21] used a bulk micromachining based approach to build such a hybrid filter for the MWIR wavelength range. The dielectric stacks were deposited onto two separate wafers and the wafers were bonded together to yield the final filter structure. The authors report that with this approach increasing the aperture of the filter requires specific considerations in stress optimization of the dielectric stack. The filters were prepared to be integrated with a single element detector. This filter has an aperture of 1.9 mm in diameter and their filter experiences warping of typically 35 nm. Antila *et. al.* [22] proposed a similar hybrid structure for the integration of a single FP filter with a detector. However, the aperture of the fabricated device was limited to 2 mm diameter and they were designed to operate with a single detector. Russin *et. al.* [23] also used a bulk micromachining based approach to build a tunable filter in the near infrared wavelength range. In order to create a large aperture for the fabricated filter they used a grid based approach where a single DBR was made of an array of mirrors. They reported a filter with 4×4 array with 200 μm mirrors and a 14×14 mirror array with 50 μm array elements. However, this approach leads to a decrease in fill factor in comparison to the same size single membrane, and places an extra design constraints on the FPA to map only optically active areas within the array of mirrors.

In this work we use bulk micromachining to open an optical path through the handle wafer. All of the suspension structures and dielectric stacks are fabricated using surface micromachining technology based on thin-film deposition and etching technologies. A conceptual diagram of such a device is shown in Fig. 1. The MEMS-based tunable optical filter consists of two distributed Bragg reflectors (DBR) separated by a half-wavelength optical cavity of air. Each DBR is a stack of alternating high and low refractive index dielectric layers, with each layer thickness being a quarter wavelength. The optical cavity between the two DBRs determines the filter peak wavelength.

An issue to address for wavelengths shorter than 1.1 μm is that silicon substrates become heavily absorbing. As such, it can be necessary for the substrate supporting the MEMS tunable filter to be etched away, to create an opening in the optically active area. We also fabricated many mm^2 size DBRs to be used to fabricate a tunable filter. The approach avoids using an array of mirrors for the DBR [23] or use of an array of individual filters per pixel [24]. Our design is based on a single large-area tunable optical filter for the entire imaging FPA.

Silicon is an excellent high refractive index material for use in the DBRs for several reasons. Firstly, the absorption characteristic of silicon allows construction of optical filters and mirrors over the entire NIR and SWIR spectral regions and beyond. Silicon is thus ideally suited to work in conjunction with InGaAs-based SWIR FPAs. Secondly, since silicon is an established MEMS structural material, the need for an additional material for support structures is eliminated, simplifying the fabrication process. Thirdly, silicon-based MEMS technology is already very mature and more cost-effective in comparison to any MEMS processes based on other materials. Taking advantage of these facts, several research groups have previously reported on the fabrication of silicon-based optical filters over the NIR to LWIR wavelength ranges [13], [25]–[28].

The technological requirements for integrating a MEMS-based tuneable optical filter to a large-area imaging FPA are:

1. The fabrication technology should be scalable to enable filters with dimensions from a few hundred microns to several millimetres, which will allow them to be integrated with either a single-element detector or with a large-area imaging FPA.
2. The optical layers must be extremely flat and free from any curvature that will otherwise degrade the peak transmission, the full width at half maximum (FWHM) of the filter, and the out-of-band rejection.
3. The filter and mirrors should have close to ideal optical performance in terms of transmittance and reflectance.
4. The large-area filter and mirrors must have a high degree of optical uniformity over the entire optically active area of the imaging FPA, in order to ensure that all pixels in the FPA receive light that has been filtered in the same manner.
5. The resonant modes of the suspended DBR mirror(s) must be mismatched to the low-frequency vibrational excitation spectrum from the environment, to ensure that the movement of the MEMS device is only due to deliberate actuation.
6. The filters need to be actuated by some well-established actuation method, such as electrostatic actuation.

In this paper we discuss solutions to the first five requirements of such a system. This work is focused on the technology to produce the essential elements of such an adaptive FPA system. This includes deposition of high optical quality dielectric materials, tuning residual stress in films by annealing, and fabrication of DBRs and fixed cavity filters with quarter-wave length thick dielectric stacks. We evaluate the high optical performance of the fabricated devices on the basis of their surface flatness, near ideal transmittance and reflectance, and their stability against any spurious low frequency vibrations. Spatially resolved optical measurements are used to demonstrate the 2-D optical uniformity of large

TABLE I
DEPOSITION PARAMETERS FOR THE SILICON OXIDE AND SILICON FILMS

Material	ICP Power (Watt)	Pressure (Pa)	Temperature (ºC)	Flow Rate (sccm)			
				SiH_4	He	N_2O	Ar
SiO_x	450	2	130	6.5	123	70	120
Si	26	4	300	6.5	123	-	-

area DBRs to be used in adaptive FPA applications. The measurement results are compared with the simulated results from optical and finite element models of fabricated devices. This paper will not address the electrostatic actuation methodology for these devices and a fully-actuated device, will be the subject of future studies.

II. EXPERIMENTAL

In this work, silicon has been used as the high refractive index material while silicon oxide (SiO_x) has been used as the low refractive index material in the DBRs. All optical layers were deposited on a 300 μm <100> oriented silicon substrate using a SENTECH SI500D inductively coupled plasma chemical vapour deposition (ICPCVD) system. An Oxford Instruments Plasmalab system 100 reactive ion etcher was used to perform low-temperature back-side etching of the substrate wafer using SF_6 and O_2 gases. This back-side etching process gives a high etch rate, vertical sidewalls, and a small degree of undercut. A Zygo Newview white light optical surface profiler was used to measure surface flatness of the suspended devices, an in-house built optical metrology system (OMS) was used to measure spatial distribution of optical performance, and a Polytec MSA 500 Micro System Analyzer was used to investigate the vibrational behavior.

III. FABRICATION PROCESS

This section describes the dielectric material growth conditions and device fabrication steps. Table I gives the deposition parameters for ICPCVD silicon oxide and silicon films. In order to measure stress in the silicon and silicon oxide films, the thin films were deposited on 70 μm thick silicon substrates. Measuring radius of curvature of the prepared samples by surface profilometry, and applying Stoney's formula [29], [30], thin film stress was calculated from stress induced substrate bowing. The as-deposited silicon thin films were found to have 560 MPa of residual compressive stress, and the as-deposited silicon oxide layer had 200 MPa of residual compressive stress.

The distributed Bragg reflectors and Fabry-Perot filters were fabricated on 300 μm thick double-side polished <100> Si substrates. A 200 nm thick SiO_x layer was deposited on the front side as an etch stop layer for the low-temperature ICPRIE back-side silicon etching process (Fig. 2 (a)). Figure 2 (b) represents two different optical structures fabricated on top of the 200 nm thick etch stop SiO_x layer. The first structure was a Si-SiO_x-Si distributed Bragg reflecting (DBR) mirror and the second structure was a Si-SiO_x-Si fixed-cavity Fabry-Perot optical filter. It is to be noted that the design

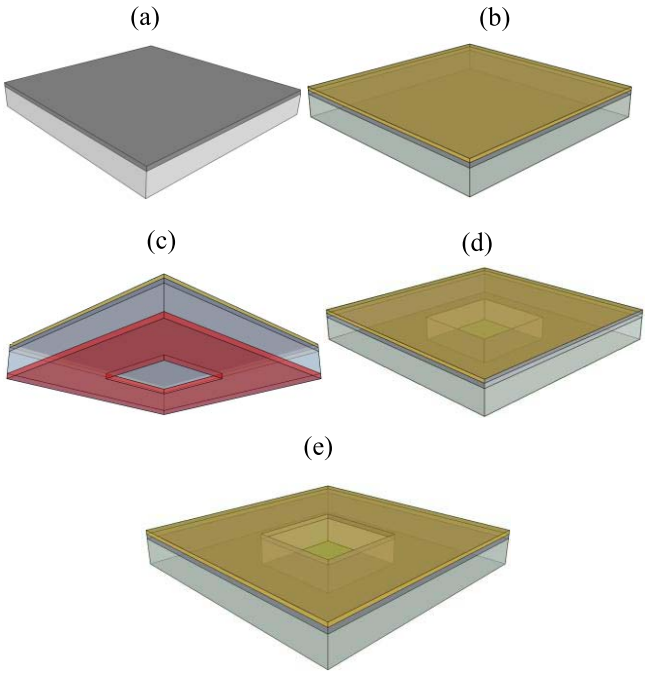

Fig. 2. Fabrication process flow of freely suspended Fabry-Perot optical filters and optical mirrors: (a) deposition of SiO_x etch stop layer (b) deposition of the optical layers (c) patterning of the back-side of the handle wafer with AZ 5214 resist (d) cryogenic back-side etching of handle wafer and removal of the AZ 5214 protective resist (e) removal of SiO_x etch stop layer in HF to leave the final suspended Fabry-Perot optical filters and DBR mirrors.

TABLE II
TARGETED AND ACTUAL THICKNESS OF THE OPTICAL LAYERS IN DIELECTRIC STACK

Layers	DBR		Filter	
	Target (nm)	Actual (nm)	Target (nm)	Actual (nm)
Si	145	136	145	150
SiO_x	360	387	714	680
Si	145	153	145	140

thickness of the optical layers was calculated for a SWIR wavelength of 2000 nm. The Si layers were targeted to have quarter-wave thickness of 145 nm. The SiOx layers were targeted to have a quarter-wave thickness for the DBR of 360 nm and a half-wave thickness of 714 nm for the Fabry-Perot filter. Table II shows the targeted and actual thickness for the optical layers.

As shown in Fig. 2 (c), AZ 5214 (positive) photoresist was patterned on the back-side of the Si substrate using a standard photolithography process. Subsequently, to achieve suspended large-area structures, a low-temperature SF_6/O_2 ICPRIE anisotropic etch with a high Si/SiO_x selectivity was used to etch through the back-side of the Si substrate (Fig. 2 (d)). In the final step shown in Fig. 2 (e), a selective HF etch was used to remove the 200 nm etch-stop SiO_x layer from the area directly beneath the final device structures.

Devices with size varying from 500 μm × 500 μm to 5 mm × 5 mm were fabricated. One such fabricated chip is shown in Fig. 3. This meets the first requirement of having a technology that can produce free-standing filters spanning

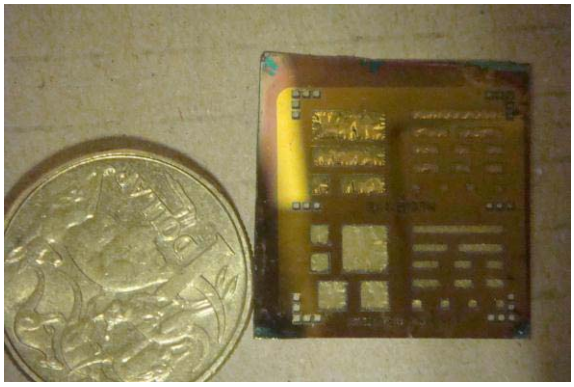

Fig. 3. Shows a Si-SiO_x-Si DBR fabricated chip before annealing. The chip has DBRs ranging in size from 500 μm × 500 μm to 5 mm × 5 mm. All the devices show significant distortions in the optical layers due to high compressive stress of Si and SiO_x films. The coin is an Australian one dollar piece of diameter of 25 mm.

the size requirements from small single-element detectors to large-area FPAs. As shown in Fig. 3, due to the compressive stress in the Si and SiO_x, the fabricated and released structures exhibited significant surface distortions, which necessitated a post-fabrication flattening process. Our previous experimental work had indicated that a post-fabrication anneal of the ICPCVD deposited Si layer was an effective means for tuning stress [31]. The fabricated structures were annealed in a quartz-tube furnace in a N_2 environment. The critical anneal temperature to convert compressive films to tensile, was approximately 350 °C. However, due to the presence of the compressively stressed SiO_x, both as an optical layer within the dielectric stack and as an etch stop layer, the critical annealing temperature of the optical structures shifted to the range of 400-420 °C. Additional studies have shown that in this temperature range the SiO_x stress is not modified, and that annealing only modifies the stress in the Si thin film layers.

IV. Optical Characterization

Optical characterization of the devices involves three types of measurements. First was optical surface profilometry to measure the flatness of fabricated devices. Second was single point transmission measurements which provides a very good indication of the quality of the optical material used to form the dielectric stacks. Third was high resolution spatial mapping of the transmission spectra. This measurement is a direct measurement of the optical transmission uniformity over the entire area, which is key to providing uniform signal to each element of a FPA, thus ensuring a high quality image with uniform spectral performance.

A. Optical Surface Profilometry of Suspended Devices

In section III it was shown that the high compressive stress generated a wrinkled surface for all fabricated devices. To achieve a high degree of flatness, the fabricated devices were annealed in a quartz tube furnace in N_2 environment. Fig. 4 shows the measured optical surface profile of a 2 mm × 1 mm suspended DBR. After annealing at 400 °C for one hour we see a total of 30 nm of bowing along the 2 mm

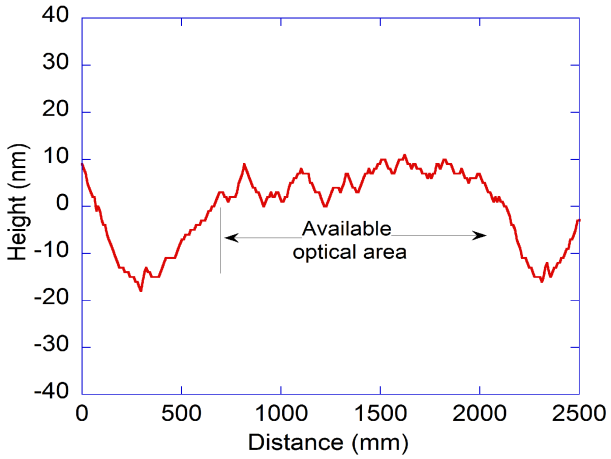

Fig. 4. Optical surface profile of a 2 mm × 1 mm suspended Si-SiO_x-Si (SiO_x = 387 nm) DBR after a 60 minute anneal at 400 °C in N_2 atmosphere. The central 1.5 mm section is flat to within 10 nm.

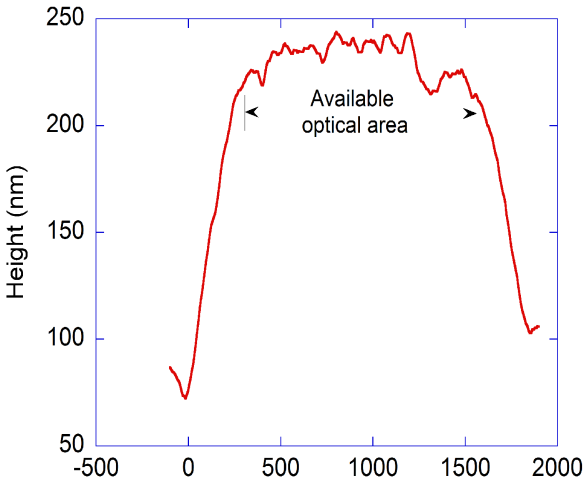

Fig. 5. Optical surface profile of a 2 mm × 1 mm suspended one-quarter wave Si-SiO_x-Si (SiO_x = 680 nm) filter after a 60 minute anneal at 420 °C in N_2 atmosphere. The central 1.25 mm section is flat to within 25 nm.

length of the DBR. The DBR is flat to within 10 nm across the 1.5 mm central portion of the 2 mm length. The remainder of the bowing is concentrated near the anchor sections where the device attaches to the substrate. The flattening of fabricated devices by annealing was observed for DBRs of all sizes and all devices were measured to be flat within 10-15 nm. This high degree of flatness is key to fabricating a tunable large area filter with two ultra-flat DBRs, which is essential to satisfying the second requirement of the process.

However we observed that the effective flat surface was approximately 75%-85% of the designed area. The decrease in the available flat area was due to bending of the membrane near the anchor sections of devices, as shown in Fig. 4. This decrease in the available optical area should be taken into account for any future studies on tunable filters.

Figure 5 shows the optical surface profile of a suspended Fabry-Perot filter of size 2 mm × 1 mm. After annealing at 420 °C for one hour in a N_2 environment, the filter shows a bowing of 220 nm along its length. This upward bowing at the

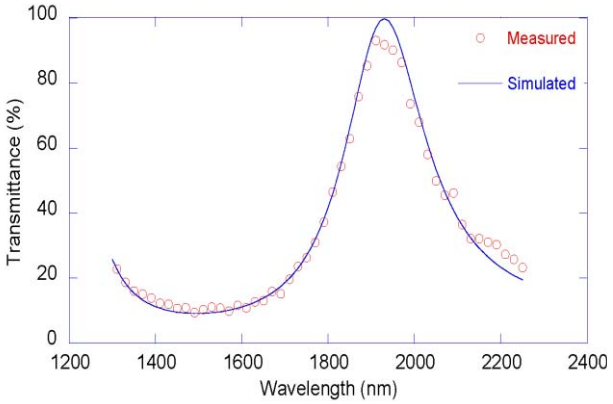

Fig. 6. Measured and simulated optical transmission spectra of the Fabry-Perot filter from Fig. 5 showing a close match between calculated and simulated transmittance.

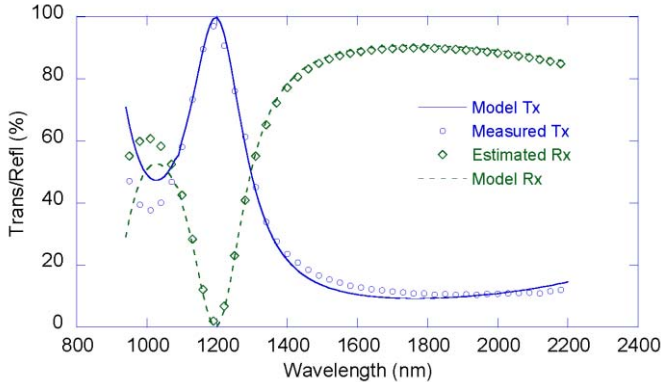

Fig. 7. Measured and model optical transmission and reflection spectra of the suspended Si-SiO_x-Si DBR from Fig. 4.

ends of the filter may be associated with the "anchor effect" caused by the stress differential between the SiO_x and Si membrane layers at the anchor location. In the central section, the filter has a flatness variation of the order of 25 nm along 1.25 mm of its length. It is noted that the fixed cavity filter shows a higher degree of bowing at the anchor in comparison to that observed at the anchors of the fabricated Si-SiO_x-Si DBRs shown in Fig. 4. This is as expected since the filters use almost double the thickness of the SiO_x in the dielectric stack, which will cause higher bowing in the fixed cavity filters. This increased bowing of the filter can be reduced by reducing the compressive stress in the silicon oxide films, however, it will require further process optimizations.

B. Single Point Transmission Spectrum of the Fabricated Mirrors and Filters

In order to meet the third requirement of the technology, that is to obtain close to theoretical optical performance, optical modelling of the mirror and filter was undertaken using the optical transfer matrix method [32]. This modelling assumed an ideal flat surface profile. The modelling result was compared to a single point measurement of the optical transmission through the structure using an in-house developed standard bench-top optical transmission measurement system.

This system enables the measurement of single point spectral transmission through the device under test at wavelengths from 600 nm to 2400 nm. The transmission was measured with the light beam focused on the device under test, to a full-width at half-maximum (FWHM) spot size of 500 μm. Fig. 6 shows the transmission spectrum of the Fabry-Perot filter whose surface profile is shown in Fig. 5. The measured spectrum indicates that the peak of the filter is at 1940 nm, which is close to the design target peak at 2000 nm. The FWHM spectral linewidth of the filter was found to be 250 nm with a peak transmission of 94% which closely matches the simulation results. This fixed cavity filter has 750 nm free spectral range (FSR) and a finesse of 3.

Figure 7 shows the single point transmittance measurement through the DBR from Fig. 4, and the model fitting to extract the reflectance. The modelled transmission profile (Model Tx) was obtained by the optical transfer matrix method assuming an ideal flat mirror profile, using previously measured optical constants of ICPCVD deposited silicon and silicon oxide films, and layer thickness measured during mirror fabrication. This model predicts a best-case reflectance (Model Rx) of 90%.

The optical transfer matrix model was also used to fit the measured transmission data (Measured T) based on the known structure of the DBR. This fit provides a better estimate of the actual thickness and optical material parameters of the layers and, as a result, provides a better estimate of the actual reflectivity (Estimated Rx) of the DBR. The measured transmission spectrum shows a peak at 1200 nm and a broad plateau above 1500 nm. From 1560 to 2050 nm the transmission is in the vicinity of 10%. The measured transmission is in good agreement with the model. The estimated reflectance is also in good agreement with the modelled reflectance. Interestingly, the mirrors have almost 90% reflectance over a 490∼nm range (1560-2050 nm), which corresponds to a 27% fractional optical bandwidth ($\Delta\lambda/\lambda$). As such, this is a good broadband reflector for use in spectroscopic imaging systems. A good agreement between measurement and model confirms the high optical quality of the Si and SiO_x films, and excellent flatness of the DBRs. With the near ideal single point optical transmittance results for the DBRs and filters the third requirement for fabricating high quality optical devices has been met.

In order to confirm the suitability of the DBRs for actuated tunable filter applications, we modelled optical transmission of a filter which is made of two such Si-SiO_x-Si based DBRs separated by a 1000 nm air cavity, which is shown in Fig. 8. The model predicts that such a filter will have 45 nm FWHM and 650 nm FSR, thus resulting in a finesse of ∼14.

C. Spatially Mapped Transmission Profile of Large-Area Quarter Wave Mirror

To meet the fourth requirement, the large area filters and mirrors must have good optical spatial uniformity over the entire optically active area. The spatial uniformity of a 3 mm × 3 mm Si-SiO_x-Si quarter-wave mirror was inves-

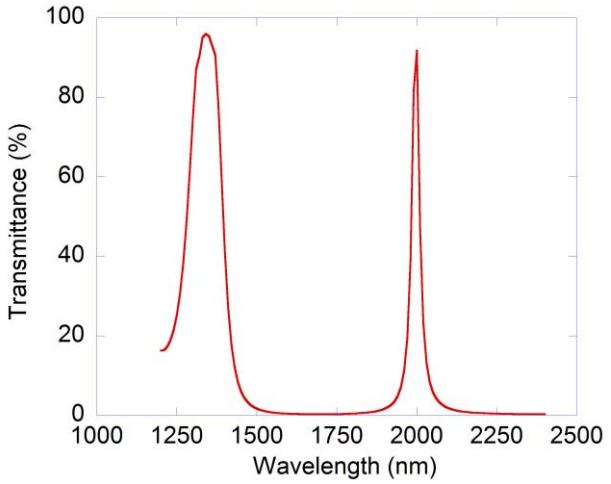

Fig. 8. Simulated optical transmission spectra for an air cavity Fabry-Perot filter made from DBRs whose reflectance are shown in Fig. 7.

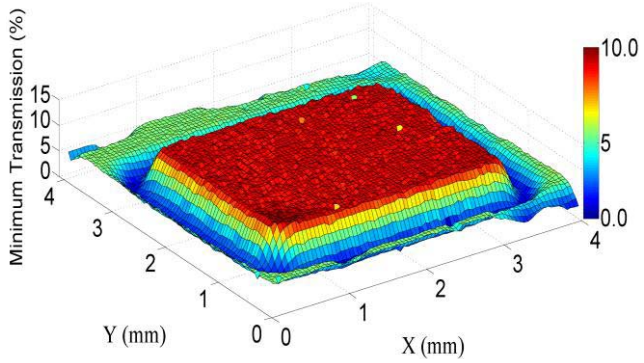

Fig. 9. Spatially resolved measurements of calibrated minimum transmission of a 3.0 mm × 3.0 mm quarter-wave Si-SiO_x-Si DBR.

tigated using an in-house developed Optical Metrology System (OMS) [33]. This system enables the mapping of calibrated transmission spectra across the full area of the mirror within the spectral band from 1400 nm to 2600 nm. The OMS measurements were carried out across a physical grid of 4.0 mm × 4.0 mm which included the 3 mm × 3 mm DBR. Fig. 9 shows the calibrated minimum transmission as a function of spatial position across the DBR surface. The light beam was focused down to a spot size of 25 μm on the mirror surface and the measurements were undertaken with a step size of 50 μm in both the X and Y directions, while the monochromator was stepped in wavelength increments of 20 nm.

The histogram of the measurement events with in the mirror surface are presented in Fig. 10 for the minimum transmission. The minimum transmission can be characterized by $\mu \pm \sigma = 0.100 \pm 0.003$, which corresponds to a 3% variation across the mirror surface for both maximum and minimum transmission. These optically homogeneous DBRs demonstrate that the fourth requirement for fabricating spatially uniform mirrors has been met.

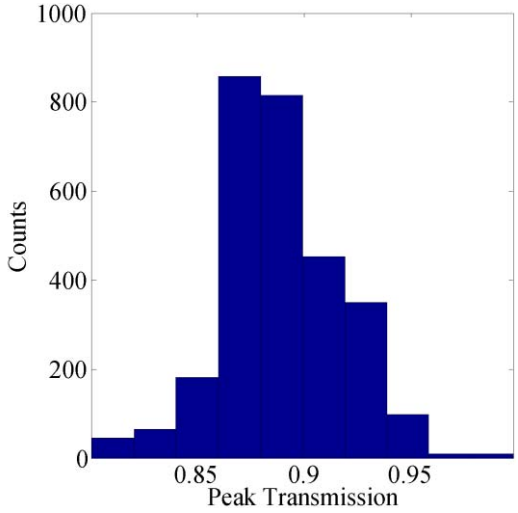

Fig. 10. Spread of minimum spectral transmission for the DBR in Fig. 9.

TABLE III
RESONANT FREQUENCIES OF 1 mm^2 SUSPENDED DBR

Mode	Finite Element Solution (kHz)	Experimental Measurement (kHz)
[1,1]	40.91	39
[1,2], [2,1]	58.63	56.5
[2,2]	73.2	68.7
[3,1], [1,3]	83	80.3
[3,2], [2,3]	94.56	93.2

V. DYNAMIC PROPERTIES OF QUARTER WAVE MIRROR

To test the mechanical robustness and utility of the optical structures for use in dynamic optical MEMS, and to assess immunity to spurious dynamic movements at low frequencies, the frequency response of the structure was measured for a 1 mm × 1 mm Si-SiO_x-Si DBR with thin films thicknesses shown in table III. The measurement setup was similar to that of [34] in which a piezoelectric stack was used as an impact hammer to excite the mirror. The resultant vibrations were measured using a vibrometer attached to an optical microscope. To eliminate air damping, the sample was mounted in an evacuated chamber at a pressure of 0.1 Torr. Suspended membrane deflection was measured with reference to the substrate in order to reduce common-mode whole-sample movement. The mechanical response of the suspended structure to the frequency sweep is shown in Fig. 11 where we identify the presence of 5 flexural resonant modes in the measurement range beginning with the fundamental vibrational mode at a frequency of 39 kHz. The low frequency resonance at 19.5 kHz is a consequence of coupling from the electronic circuitry. These measurements were corroborated with a finite element simulation of natural resonant frequencies of the suspended mirror using CoventorWare 2010 MEMS design suite [35]. The mechanical properties of the silicon and silicon oxide thin films were measured and used as an input to the simulated model. The results on modal response are summarized in the table III which also compares the finite element modelling results with the experimental obser-

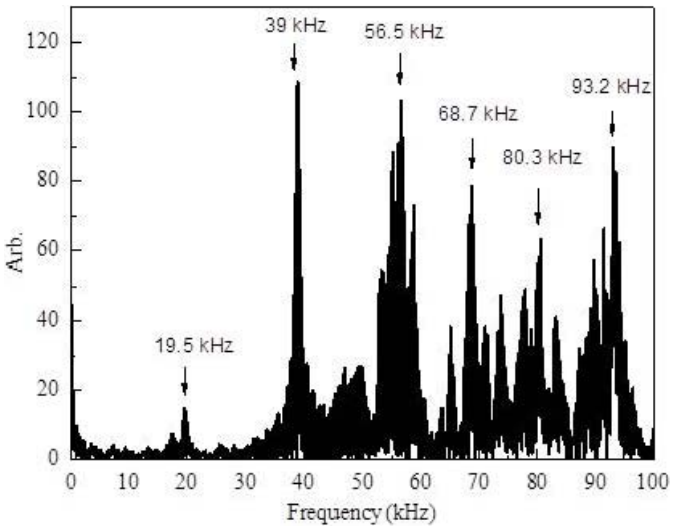

Fig. 11. Measured flexural modes of 1 mm × 1 mm suspended one quarter wave Si-SiO_x-Si DBR showing the fundamental and harmonic flexural modes.

vations. The model indicates that in the 10 kHz to 100 kHz frequency range, five modes of vibration are present, where the fundamental mode [1, 1] occur at approximately 40 kHz. Other modes and natural frequencies are also indicated in Table III, and it is noted that the modelled results and experimental measurements are in general agreement within approximately 5%. These variations can be attributed to the measurement accuracy of the material properties. A high fundamental frequency value of 39 kHz suggests a predictable and fast dynamic response of the optical structure combined with immunity to low frequency stimuli from spurious external vibrations.

VI. Conclusion

In this paper we have presented the design and associated fabrication process to realise large area Si-SiO_x based suspended optical structures with size varying from 500 μm × 500 μm to 5 mm × 5 mm. These suspended structures can be used to fabricate tunable Fabry-Perot optical filters in conjunction with either single-element detectors or large-area imaging FPAs. The optimization process of the optical and mechanical properties of the ICPCVD deposited thin films yielded excellent flatness and uniform optical properties over the optically active area of the suspended structures. Post-fabrication annealing of the filters and mirrors was employed to achieve very-flat optical surface profiles for both filters and DBRs. The single point optical measurement indicates an excellent match with the simulation model, providing further evidence for the high quality of the optical thin films and near-ideal performance of the Fabry-Perot cavity. We have also presented 2-D spatially resolved optical measurements with minimum transmission $\mu \pm \sigma = 0.100 \pm 0.003$. The presented technology demonstrates that over many square millimeters in area the variation in optical characteristics was less than 3% providing further evidence as to the excellent spatial uniformity of the suspended structures. Finally, measured and simulated dynamic characteristics of the membranes have been presented, indicating their effectiveness to be employed as dynamic optical MEMS devices, and providing a high level of immunity to external low frequency vibrations.

References

[1] B. M. Onat, W. Huang, N. Masaun, M. Lange, M. H. Ettenberg, and C. Dries, "Ultra-low dark current InGaAs technology for focal plane arrays for low-light level visible-shortwave infrared imaging," *Proc. SPIE*, vol. 6542, pp. 65420L-1–65420L-9, Apr. 2007.

[2] A. D. Hood, M. H. MacDougal, J. Manzo, D. Follman, and J. C. Geske, "Large-format InGaAs focal plane arrays for SWIR imaging," *Proc. SPIE*, vol. 8353, p. 83530A, May 2012.

[3] T. J. Martin, M. J. Cohen, J. C. Dries, and M. J. Lange, "InGaAs/InP focal plane arrays for visible light imaging," *Proc. SPIE*, vol. 5406, pp. 38–45, Aug. 2004.

[4] T. R. Hoelter and J. B. Barton, "Extended short-wavelength spectral response from InGaAs focal plane arrays," *Proc. SPIE*, vol. 5074, pp. 481–490, Sep. 2003.

[5] E. N. Lewis *et al.*, "Fourier transform spectroscopic imaging using an infrared focal-plane array detector," *Anal. Chem.*, vol. 67, no. 19, pp. 3377–3381, 1995.

[6] P. J. Treado, E. N. Lewis, and I. W. Levin, "Near-infrared acousto-optic filtered spectroscopic microscopy: A solid-state approach to chemical imaging," *Appl. Spectrosc.*, vol. 46, no. 4, pp. 553–559, 1992.

[7] H. Koç, V. W. Smail, and D. L. Wetzel, "Reliability of InGaAs focal plane array imaging of wheat germination at early stages," *J. Cereal Sci.*, vol. 48, no. 2, pp. 394–400, 2008.

[8] C. B. Singh, D. S. Jayas, J. Paliwal, and N. D. G. White, "Detection of insect-damaged wheat kernels using near-infrared hyperspectral imaging," *J. Stored Prod. Res.*, vol. 45, no. 3, pp. 151–158, 2008.

[9] R. C. Lyon *et al.*, "Near-infrared spectral imaging for quality assurance of pharmaceutical products: Analysis of tablets to assess powder blend homogeneity," *AAPS PharmSciTech*, vol. 3, no. 3, pp. 1–15, 2002.

[10] R. D. Driver and K. Didona, "Online high-speed NIR diffuse-reflectance imaging spectroscopy in food quality monitoring," *Proc. SPIE*, vol. 7351, pp. 73150J-1–73150J-8, Apr. 2008.

[11] P. J. Treado, I. W. Levin, and E. N. Lewis, "Indium antimonide (InSb) focal plane array (FPA) detection for near-infrared imaging microscopy," *Appl. Spectrosc.*, vol. 48, no. 5, pp. 607–615, 1994.

[12] R. A. Crocombe, "Miniature optical spectrometers: There's plenty of room at the bottom part I, background and mid-infrared spectrometers," *Spectroscopy*, vol. 23, no. 1, p. 38, 2008.

[13] D. Rossberg, "Silicon micromachined infrared sensor with tunable wavelength selectivity for application in infrared spectroscopy," *Sens. Actuators A, Phys.*, vol. 47, nos. 1–3, pp. 413–416, 1995.

[14] R. F. Wolffenbuttel, "State-of-the-art in integrated optical microspectrometers," *IEEE Trans. Instrum. Meas.*, vol. 53, no. 1, pp. 197–202, Feb. 2004.

[15] L. P. Schuler, J. S. Milne, J. M. Dell, and L. Faraone, "MEMS-based microspectrometer technologies for NIR and MIR wavelengths," *J. Phys. D, Appl. Phys.*, vol. 42, no. 13, p. 133001, 2009.

[16] J. S. Milne, J. M. Dell, A. J. Keating, and L. Faraone, "Widely tunable MEMS-based Fabry–Pérot filter," *J. Microelectromech. Syst.*, vol. 18, no. 4, pp. 905–913, Aug. 2009.

[17] C. A. Musca *et al.*, "Monolithic integration of an infrared photon detector with a MEMS-based tunable filter," *IEEE Electron Device Lett.*, vol. 26, no. 12, pp. 888–890, Dec. 2005.

[18] A. J. Keating, K. K. M. B. D. Silva, J. M. Dell, C. A. Musca, and L. Faraone, "Optical characterization of Fabry–Pérot MEMS filters integrated on tunable short-wave IR detectors," *IEEE Photon. Technol. Lett.*, vol. 18, no. 9, pp. 1079–1081, May 1, 2006.

[19] N. Quack, S. Blunier, J. Dual, F. Felder, M. Arnold, and H. Zogg, "Mid-infrared tunable resonant cavity enhanced detectors," *Sensors*, vol. 8, no. 9, pp. 5466–5478, 2008.

[20] F. Felder, M. Arnold, M. Rahim, C. Ebneter, and H. Zogg, "Tunable lead-chalcogenide on Si resonant cavity enhanced midinfrared detector," *Appl. Phys. Lett.*, vol. 91, no. 10, p. 101102, 2007.

[21] N. Neumann, M. Ebermann, S. Kurth, and K. Hiller, "Tunable infrared detector with integrated micromachined Fabry–Pérot filter," *J. Microlithograph. Microfabrication Microsyst.*, vol. 7, no. 2, p. 9, 2008.

[22] J. Antila *et al.*, "MEMS and piezo actuator-based Fabry–Pérot interferometer technologies and applications at VTT," *Proc. SPIE*, vol. 7680, pp. 76800U-1–76800U-12, Apr. 2010.
[23] T. J. Russin, M. Kerber, A. Russin, A. Wang, and R. Waters, "Fabrication and analysis of a MEMS NIR Fabry–Pérot interferometer," *J. Microelectromech. Syst.*, vol. 21, no. 1, pp. 181–189, 2012.
[24] J. S. Milne, "Micro-electromechanical technologies for next-generation spectroscopic systems," Ph.D. dissertation, School Electron., Elect. Comput. Eng., Univ. Western Australia, Crawley, Australia, 2009.
[25] A. Lipson and E. M. Yeatman, "A 1-D photonic band gap tunable optical filter in (110) silicon," *J. Micromech. Syst.*, vol. 16, no. 3, pp. 521–527, 2007.
[26] D. Cristea, M. Kusko, C. Tibeica, R. Muller, E. Manea, and D. Syvridis, "Design and experiments for tunable optical sensor fabrication using (111)-oriented silicon micromachining," *Sens. Actuators A, Phys.*, vol. 113, no. 3, pp. 312–318, 2004.
[27] B. Saadany, M. Malak, F. Marty, Y. Mita, D. Khalil, and T. Bourouina, "Electrostatically-tuned optical filter based on silicon Bragg reflectors," presented at the IEEE/LEOS International Optical MEMS Applications Conference, Big Sky, MT, USA, 2006.
[28] M. Tuohiniemi, M. Blomberg, A. Akujärvi, J. Antila, and H. Saari, "Optical transmission performance of a surface-micromachined Fabry–Pérot interferometer for thermal infrared," *J. Micromech. Microeng.*, vol. 22, no. 11, p. 115004, 2012.
[29] G. G. Stoney, "The tension of metallic films deposited by electrolysis," *Proc. Roy. Soc. London Ser. A, Contain. Papers Math. Phys. Character*, vol. 82, no. 553, pp. 172–175, 1909.
[30] X. Feng, Y. Huang, and A. J. Rosakis, "On the Stoney formula for a thin film/substrate system with nonuniform substrate thickness," *J. Appl. Mech.*, vol. 74, no. 6, pp. 1276–1281, 2007.
[31] D. K. Tripathi *et al.*, "A silicon based surface micro-machined distributed Bragg reflector for MEMS spectroscopic applications," in *Proc. 8th IEEE ICIIS*, Kandy, Sri Lanka, Dec. 2013, pp. 289–293.
[32] H. A. Macleod, *Thin-Film Optical Filters*. New York, NY, USA: McGraw-Hill, 1989.
[33] R. Rafiei *et al.*, "A versatile instrumentation system for MEMS-based device optical characterization," *Proc. SPIE*, vol. 8923, pp. 89232V-1–89232V-9, Dec. 2013.
[34] H.-C. Tsai and W. Fang, "Determining the Poisson's ratio of thin film materials using resonant method," *Sens. Actuators A, Phys.*, vol. 103, no. 3, pp. 377–383, 2003.
[35] CoventorWare. [Online]. Available: http://www.coventor.com/mems-solutions/products/coventorware/, accessed Oct. 15, 2014.

Dhirendra Kumar Tripathi received the B.Tech. degree in electronics engineering from Uttar Pradesh Technical University, Lucknow, India, and the M.Tech. degree in very large scale integration systems from NIT, Trichy, India, in 2005 and 2008, respectively. He is currently pursuing the Ph.D. degree with the School of Electrical, Electronic, and Computer Engineering, University of Western Australia, Perth, WA, Australia. His current research activities involve in design and fabrication of optical microelectromechanical systems (MEMS) devices and materials for MEMS.

Fei Jiang was born in China in 1983. He received the B.E. and M.A. degrees in materials science from the Harbin University of Science and Technology, Harbin, China, in 2005 and 2008, respectively, and the Ph.D. degree in electrical and electronic engineering and mechanical engineering from the University of Western Australia (UWA), Perth, WA, Australia, in 2008.

He was a Graduate Research Assistant with UWA. His research activities are in the fields of micro-electromechanical systems (MEMS) actuators and optical MEMS spectrometers. He is currently with MRX Technologies, West Perth, WA, Australia.

Ramin Rafiei is currently an Associate Professor of Microelectronics Engineering with the University of Western Australia, Perth, WA, Australia, where he is involved in research on optical microelectromechanical systems. Prior to this appointment, he was with the Australian Nuclear Science and Technology Organization, Lucas Heights, NSW, Australia, where he led an international collaboration on the development of advanced compound semiconductor radiation detectors for medical imaging and in-field radiological threat detection. He received the Ph.D. degree in experimental nuclear physics from Australian National University, Canberra, ACT, Australia. He was a recipient of the University Medal in both engineering and physics. Prior to his Ph.D. studies, he was an Engineer with Ford Motors, Geelong, VIC, Australia, and Boeing Defence, Brisbane, QLD, Australia.

K. K. M. B. Dilusha Silva was born in Sri Lanka in 1973. He received the Hons. degrees in physics and electronics engineering from the University of Western Australia (UWA), Perth, WA, Australia, and the Ph.D. degree in optical imaging technologies for biomedical applications in 2004. He has been with industry and academia, and is currently a Research Professor and the Engineering Manager with the Microelectronics Research Group, UWA. Since returning to UWA in 2009, his research interests include in optical microelectromechanical systems (MEMS) sensors, optical spectroscopic sensors, and MEMS biosensors. He has attracted funding for his research from the agriculture and aerospace sectors, and the government, and also leads a number of MEMS related research efforts at MRG, with strong commercial links to both the agricultural and aerospace sectors.

Jarek Antoszewski received the Master's degree in physics from Teachers College in Olsztyn, Olsztyn, Poland, in 1977, and the Ph.D. degree in semiconductor physics from the Institute of Physics of Polish Academy of Science, Warsaw, Poland, in 1982. From 1982 to 1990, he was a Researcher and then a Project Leader with the Research and Development Laboratory, WILMER Ltd., Warsaw, where he was involved in design and testing of infrared radiometers for industrial applications. In 1991, he joined the Microelectronics Research Group, University of Western Australia, Perth, WA, Australia, where he has been involved in magneto-transport studies of semiconductor materials, and physics and technology of infrared detectors. His current research interests include the development of technology merging II–VI and III–V-based infrared detectors with microelectromechanical systems technology into a new technology for monolithic and tunable infrared sensors.

Mariusz Martyniuk was born in Poland in 1976. He received the B.Sc. (Hons.) degree from the University of Toronto, ON, Canada; the M.A.Sc. degree from McMaster University, Hamilton, ON, and the Ph.D. degree from the University of Western Australia (UWA), Perth, WA, Australia, in 2007.

He worked in the industry sector as an Electronics Engineer before rejoining UWA, where he is currently a Research Professor with the Microelectronics Research Group and manages the Western Australian Node of the Australian National Fabrication Facility. His primary areas of interest encompass thin-film materials and thin-film mechanics, and their applications in microelectromechanical systems and optoelectronic devices.

Dr. Martyniuk's research contributions were recognized by the Award of the Inaugural Australian Museum Eureka Prize (the Oscars of Australian Science) for Outstanding Science in Support of Defence or National Security in 2008.

John M. Dell is currently a Professor of Electrical Engineering with the University of Western Australia, Perth, WA, Australia.

His primary areas of interest are semiconductor optoelectronics and optical microelectromechanical systems devices. He has been with the industry and academia in these fields. Work undertaken by his group on robust and low-cost microspectrometer technology has attracted funding from the U.S. and the Australian Department of Defence, and more recently from the Australian Grains Research and Development Corporation. This latter funding is for the development of low-cost tools using infrared spectroscopy for broad acre agriculture applications. This work is being undertaken as a collaboration between Electrical Engineers and Soil Scientists. He has several patents, and over 200 journal and conference publications.

Lorenzo Faraone was born in Italy in 1951. He received the Ph.D. degree from the University of Western Australia (UWA), Perth, WA, Australia, in 1979.

He was a Research Scientist with Lehigh University, Bethlehem, PA, USA, from 1979 to 1980, where he was involved in studies on MOS devices. From 1980 to 1986, he was a Member of the Technical Staff with RCA Laboratories, David Sarnoff Research Center, Princeton, NJ, USA, where he was involved in very large scale integration CMOS and nonvolatile memory technologies, and space radiation effects in silicon-on-sapphire MOS integrated circuits. He joined the School of Electrical, Electronic, and Computer Engineering, UWA, in 1987, where he has been a Professor since 1998, and the Head of the Department/School of Electrical, Electronic, and Computer Engineering from 1999 to 2003. Since his arrival at UWA, his research interests have been in the area of compound semiconductor materials and devices, and microelectromechanical systems (MEMS). In particular, his interests include mercury cadmium telluride materials and device technologies for infrared detector arrays, gallium nitride technology for ultraviolet detectors and high-speed/high-power electronics, and MEMS technologies for tunable optical cavity infrared detectors. He currently holds over 10 U.S. patents, has supervised over 25 Ph.D. student completions, and authored over 300 refereed technical papers in journals and conference proceedings.

Prof. Faraone was a recipient of the RCA Laboratories Individual Outstanding Achievement Award in 1983 and 1986, and the John de Laeter Innovation Award in 1997.